

Eq.Bot: Enhance Robotic Manipulation Learning via Group Equivariant Canonicalization

Jian Deng¹, Yuandong Wang^{1†}, Yangfu Zhu¹, Tao Feng², Tianyu Wo³, Zhenzhou Shao^{1†}

¹Beijing Key Laboratory of Light Industrial Robot and Safety Verification, Capital Normal University

²Department of Computer Science and Technology, Tsinghua University

³School of Software, Beihang University

†Corresponding authors: wangyd@cnu.edu.cn, zshao@cnu.edu.cn

Abstract

Robotic manipulation systems are increasingly deployed across diverse domains. Yet existing multi-modal learning frameworks lack inherent guarantees of geometric consistency, struggling to handle spatial transformations such as rotations and translations. While recent works attempt to introduce equivariance through bespoke architectural modifications, these methods suffer from high implementation complexity, computational cost, and poor portability. Inspired by human cognitive processes in spatial reasoning, we propose **Eq.Bot**, a universal canonicalization framework grounded in $SE(2)$ group equivariant theory for robotic manipulation learning. Our framework transforms observations into a canonical space, applies an existing policy, and maps the resulting actions back to the original space. As a model-agnostic solution, **Eq.Bot** aims to endow models with spatial equivariance without requiring architectural modifications. Extensive experiments demonstrate the superiority of **Eq.Bot** under both CNN-based (e.g., CLIPort) and Transformer-based (e.g., OpenVLA-OFT) architectures over existing methods on various robotic manipulation tasks, where the most significant improvement can reach 50.0%.

1. Introduction

Robotic manipulation has become a fundamental technology across diverse domains, from industrial automation to service robotics [26]. A fundamental challenge in this field involves handling arbitrary spatial transformations (such as translations and rotations), which introduce large uncertainty to robot operation [22]. Conventional learning-based frameworks often exhibit limited robustness to these geometric variations, typically relying on large-scale datasets to implicitly learn transformation patterns [33]. These data-intensive approaches incur substantial costs in both data col-

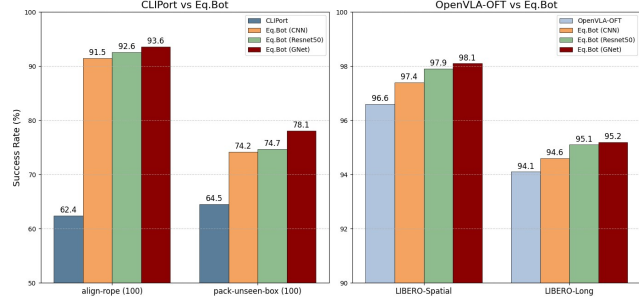


Figure 1. Performance comparison on Robotic Manipulation Benchmarks. Our model-agnostic framework significantly boosts the performance of both the CNN-based CLIPort (left) and the Transformer-based OpenVLA-OFT (right). On the pack-unseen-box task (demo = 100), Eq.Bot improves CLIPort’s success rate from 62.4% to 93.6%. For OpenVLA-OFT, our method consistently enhances performance on the LIBERO benchmarks.

lection and training, yet still fail to provide systematic guarantees for generalization of novel tasks [9].

Recent advances in multi-modal learning have demonstrated great progress in robotic manipulation. CNN-based [18] architectures like CLIPORT [34] effectively fuse visual and linguistic information, while Transformer-based Vision-Language-Action (VLA) models [39] such as OpenVLA-OFT [20] generate actions from tokenized observations and language instructions, exhibiting strong generalization capabilities across diverse tasks. However, these systems lack inherent equivariance guarantees: when inputs undergo spatial transformations, their outputs fail to transform predictably. Contemporary approaches have begun addressing this limitation. GEM [16] introduces equivariance into CLIPORT through textual-visual relevancy maps and language-steerable kernels, while Transformer-centric methods like EquAct [42] achieve continuous $SE(3)$ equivariance by combining an $SE(3)$ -equivariant point-cloud U-Net (utilizing spherical Fourier features) with invariant

iFiLM layers for language conditioning, ensuring both equivariant keyframe predictions and instruction invariance under 3D transformations. Nevertheless, these methods necessitate substantial architectural redesign, significantly increasing implementation complexity and reducing portability across different backbone architectures.

The core insight of our approach is that spatial transformations in manipulation tasks inherently obey equivariance principles, which can be systematically formalized within the group equivariant theory [23]. This enables models to learn essential geometric relationships without requiring exhaustive training data covering all possible spatial variations. Furthermore, inspired by human cognitive processes during manipulation of spatially transformed objects [32], humans intuitively map objects into a mental "canonical space," execute actions within this standardized representation, and subsequently transform results back to the physical space. This cognitive paradigm not only reinforces the practical relevance of equivariance but also suggests a computationally efficient strategy that can be rigorously formalized using group-theoretic principles.

In this paper, we address the spatial transformation challenge through a comprehensive theoretical analysis of existing multimodal frameworks from the group equivariant perspective. Considering the portability and reliability, we present **Eq.Bot**, a universal canonicalization framework grounded in SE(2) group equivariant theory for **robotic** manipulation learning. We rigorously establish the theoretical foundations for applying SE(2) equivariance to robotic manipulation, which enhances the theoretical basis of **Eq.Bot**. Meanwhile, our proposed **Eq.Bot** can also be seamlessly integrated into existing multimodal architectures as a plug-in component. Moreover, the performance gain of our framework is very impressive on most of the evaluated robotic manipulation tasks. As shown in Figure 1, **Eq.Bot** promotes the success rate of CLIPort from 62.4% to 93.6%, about 50.0% improvement, which means a lot for robotic manipulation learning.

Our main contributions are: (1) A systematic theoretical analysis of equivariance deficiencies in current multimodal robotic learning frameworks and rigorous proof of group theory foundations for robotic manipulation; (2) A universal, model-agnostic canonicalization framework providing spatial generalization enhancement without architectural modifications; and (3) Comprehensive experimental validation under different backbone architectures on various robotic manipulation tasks, demonstrating superior performance and robustness of our solution.

2. Preliminaries

This section introduces the mathematical foundations for group theory, and theoretically analyzes the equivariance deficiencies in current existing multi-modal architectures.

The Fundamentals of Group Theory. Group theory [11] provides the mathematical framework for understanding symmetries and transformations in robotic manipulation. A group (G, \circ) consists of a set G with a binary operation \circ satisfying four fundamental axioms: 1) closure ($g_1 \circ g_2 \in G$), 2) associativity ($((g_1 \circ g_2) \circ g_3 = g_1 \circ (g_2 \circ g_3))$), 3) identity element existence ($e \circ g = g \circ e = g$), and 4) inverse element existence ($g \circ g^{-1} = g^{-1} \circ g = e$).

Group actions [19] provide the foundation for describing how spatial transformations systematically affect both visual observations and corresponding optimal actions. A group action $\cdot : G \times X \rightarrow X$ satisfies identity preservation ($e \cdot x = x$) and composition compatibility ($((g_1 \circ g_2) \cdot x = g_1 \cdot (g_2 \cdot x))$).

Equivariant Mappings. Let G be a group acting on X and Y , for all $g \in G$ and $x \in X$, a function $f : X \rightarrow Y$ is equivariant if:

$$f(\rho(g) \cdot x) = \rho'(g) \cdot f(x), \quad (1)$$

This fundamental property ensures that the function's output transforms predictably when the input undergoes a group transformation, providing a mathematical guarantee of consistent behavior under symmetries. While invariance requires $f(g \cdot x) = f(x)$, where output remains unchanged under transformations, equivariance allows output to transform according to the group action: $f(g \cdot x) = \rho(g) \cdot f(x)$.

The Equivariance Analysis of Existing Multi-modal Models. Formally, for any transformation $g \in G$ with corresponding representations ρ_X and ρ_A acting on the input and output spaces, a policy $\pi : \mathcal{X} \rightarrow \mathcal{A}$ is G -equivariant, if:

$$\pi(\rho_X(g) \cdot x) = \rho_A(g) \cdot \pi(x). \quad (2)$$

1) *Equivariance Deficiencies in CNN-based Architectures (CLIPort):* the policy π_{CLIPort} suffers from systematic equivariance deficiencies across its architectural components. The semantic stream f_{sem} , typically a pre-trained CLIP encoder, is fundamentally non-equivariant due to standard CNN operations like pooling and strided convolutions that break geometric structure [4]. For an input image I and a rotation $g \in SO(2)$:

$$f_{\text{sem}}(g \cdot I) \neq \rho_{\text{feat}}(g) \cdot f_{\text{sem}}(I), \quad (3)$$

where ρ_{feat} represents the group action in feature space.

The spatial stream f_{spat} exhibits only partial equivariance. As established by Kaba et al. [14], while the placing network achieves discrete $SO(2)$ equivariance through explicit rotation correlation, the picking network remains merely translation-equivariant due to its argmax-based selection mechanism. This architectural asymmetry prevents full spatial stream equivariance.

The fusion operation f_{fusion} definitively breaks the equivariance chain. It combines the non-equivariant semantic vector z_{sem} with the spatial feature map F_{spat} through

element-wise multiplication:

$$F_{\text{fused}} = F_{\text{spat}} \odot \text{Broadcast}(z_{\text{sem}}), \quad (4)$$

When the input is rotated, the spatial stream produces $\rho_{\text{spat}}(g) \cdot F_{\text{spat}}$, but the semantic stream yields an unpredictable $z'_{\text{sem}} = f_{\text{sem}}(g \cdot I)$ unrelated to z_{sem} . The resulting fused representation:

$$F'_{\text{fused}} = (\rho_{\text{spat}}(g) \cdot F_{\text{spat}}) \odot \text{Broadcast}(z'_{\text{sem}}), \quad (5)$$

cannot equal the correctly transformed $\rho_{\text{spat}}(g) \cdot F_{\text{fused}}$ due to the semantic mismatch. This corruption at the fusion systematically undermines the policy's geometric consistency.

2) *Equivariance Deficiencies in Transformer-based Architectures (OpenVLA-OFT)*: the systematic equivariance deficiencies of policy $\pi_{\text{OpenVLA-OFT}}$ rooted in transformer architecture. The patch tokenization operation discretizes the continuous image space into fixed grid positions, destroying the continuous group structure essential for equivariance:

$$\begin{aligned} f_{\text{vit}}(g \cdot I) &= \text{Transformer}(\text{Patches}(g \cdot I) + P) \\ &\neq \rho_{\text{feat}}(g) \cdot f_{\text{vit}}(I), \end{aligned} \quad (6)$$

where $P \in \mathbb{R}^{N \times D}$ represents the fixed positional encodings that are invariant to input transformations.

The standard self-attention mechanism further exacerbates this deficiency. The attention are computed based on absolute positional relationships rather than relative geometric transformations:

$$A(g \cdot I)_{ij} \neq A(I)\rho(g)^{-1}(i)\rho(g)^{-1}(j), \quad (7)$$

This hinders the equivariance property since the attention pattern does not transform predictably with the input.

The action decoder f_{decoder} maps the transformer's output embeddings to continuous actions through learned linear projections:

$$f_{\text{decoder}}(g \cdot I, z_{\text{text}}) \neq \rho_{\mathcal{A}}(g) \cdot f_{\text{decoder}}(I, z_{\text{text}}). \quad (8)$$

This final mapping lacks the geometric structure necessary to preserve equivariance, as the decoder weights are fixed and do not transform with input rotations.

These systematic deficiencies across architectural paradigms necessitate architecture-agnostic solutions that enhance spatial equivariance while preserving existing representational strengths.

3. Method

We consider the fundamental challenge of learning robust manipulation policies from multi-modal demonstrations in the presence of spatial transformations. Given a dataset of demonstrations $\mathcal{D} = (I_i, \ell_i, A_i)_{i=1}^N$, where $I_i \in \mathbb{R}^{H \times W \times 3}$

represents a set of images at several camera views, ℓ_i denotes natural language instructions that specify the task, and A_i represents robotic manipulation actions, the objective is to learn a policy $\pi : (I, \ell) \rightarrow A$ that generalizes robustly across diverse spatial configurations. The core challenge lies in developing architectures that can maintain consistent manipulation performance when objects undergo arbitrary rotations and translations, while preserving the inherent representational strengths of existing multi-modal frameworks.

3.1. The Proposed Universal Eq.Bot Framework

Drawing inspiration from cognitive psychology research on human spatial reasoning, we formalize this cognitive process into a computational framework. Given an existing policy π_{base} , the equivariant policy is constructed as:

$$\pi_{\text{canon}}(I, \ell) = g_{\text{canon}}^{-1} \cdot \pi_{\text{base}}(C(I), \ell), \quad (9)$$

where $C : I \rightarrow I_{\text{canon}}$ represents the canonicalization function that transforms observations to a canonical orientation, and g_{canon} denotes the corresponding transformation.

As shown in Figure 2, the framework operates through three stages that ensure spatial equivariance across diverse architectures. The input observation I first undergoes canonicalization through our group equivariant network:

$$(I_{\text{canon}}, g_{\text{est}}) = C(I), \quad (10)$$

where g_{est} denotes the estimated transformation parameters. The canonicalized observation is then processed through a base manipulation policy π_{base} to generate action predictions in the canonical coordinate system:

$$A_{\text{canon}} = \pi_{\text{base}}(I_{\text{canon}}, \ell). \quad (11)$$

Finally, the canonical actions undergo inverse transformation to restore original coordinate alignment:

$$A_{\text{final}} = g_{\text{est}}^{-1} \cdot A_{\text{canon}}. \quad (12)$$

This model-agnostic design enables our framework to seamlessly integrate with both CNN-based systems (e.g., CLIPORT) and Transformer-based models (e.g., OpenVLA-OFT) without requiring substantial architectural modifications, providing a universal solution for spatial equivariance in robotic manipulation.

3.2. Group Equivariant Canonicalization Network

The group equivariant canonicalization network serves as the core component of our framework, systematically transforming arbitrary input observations into a standardized canonical orientation. Inspired by recent work on equivariant learning [17], our framework accommodates both equivariant and non-equivariant network architectures to perform canonicalization, including three distinct network implementations, each presenting distinct trade-offs between computational efficiency and representational capacity.

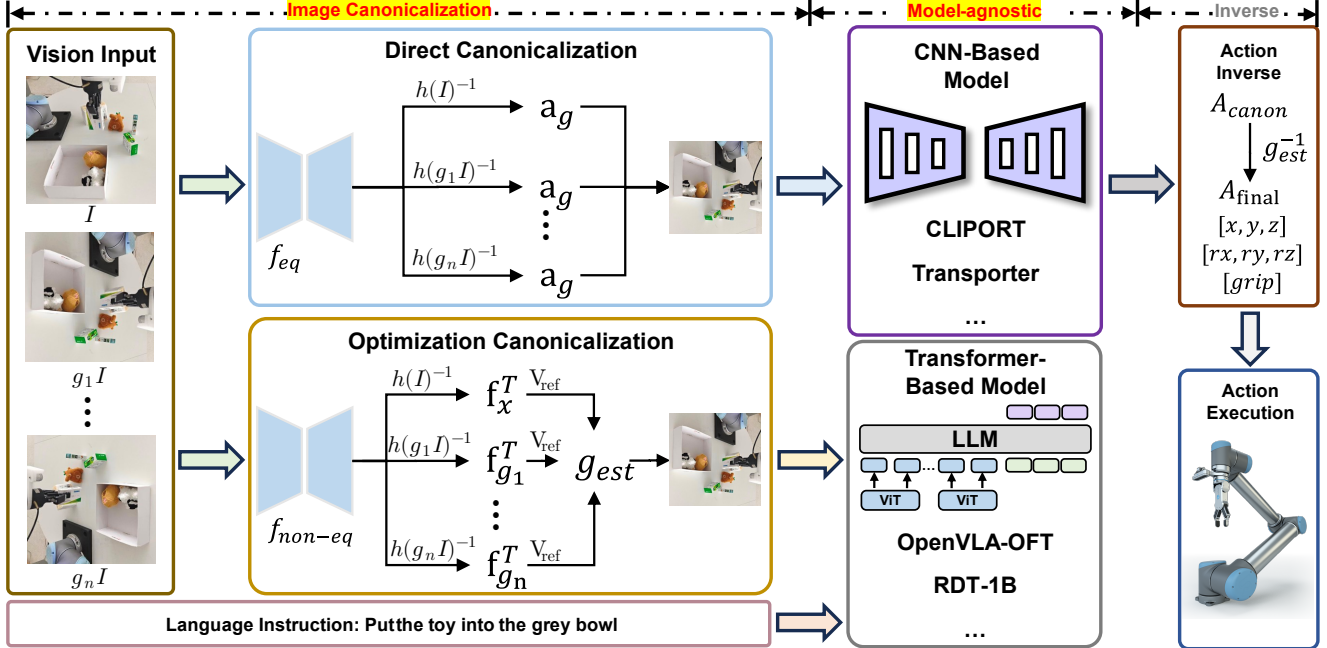


Figure 2. Overview of the proposed Eq.Bot framework, a model-agnostic solution that enhances spatial equivariance to existing manipulation systems. Grounded in equivariant theory, Eq.Bot introduces a canonicalization process that transforms input observations into standardized canonical orientations. These canonicalized observations are then fed into an unmodified base policy (e.g., CLIPort or OpenVLA) to generate actions. Finally, the resulting actions are mapped back to the original space through inverse transformation for execution.

Canonicalization Process. While the framework is compatible with arbitrary discrete rotation groups, we focus our exposition on the cyclic group C_4 , which effectively models the 90-degree rotational symmetries prevalent in tabletop manipulation tasks. As illustrated in Figure 2, the process commences by generating the complete orbit of an input observation $I \in \mathbb{R}^{H \times W \times 3}$ under the action of C_4 :

$$\begin{aligned} \mathcal{T} &= \{g \cdot I : g \in C_4\} \\ &= \{I, R_{90^\circ} \cdot I, R_{180^\circ} \cdot I, R_{270^\circ} \cdot I\}, \end{aligned} \quad (13)$$

where R_θ denotes rotation by angle θ . Then, all the transformed images are fed into a canonicalization network to obtain the optimal canonical direction. The canonicalized observation is obtained through inverse transformation:

$$I_{\text{canon}} = g_{\text{est}}^{-1} \cdot I. \quad (14)$$

This inverse operation rotates the input observation by the negative of the estimated canonical angle, effectively aligning it with the learned canonical orientation.

Equivariant Network (Direct Canonicalization). The equivariant architecture, denoted as f_{eq} in Figure 2, is instantiated as a Group Equivariant CNN (G-CNN) through the E2CNN framework [37]. This network is inherently equivariant to the actions of a discrete group, such as C_4 . When presented with the orbit of an input image,

$g \cdot I \mid g \in C_4$, the f_{eq} leverages its constrained convolutional filters to produce structured feature maps that transform predictably with the input. This allows the network to directly infer the canonical orientation by identifying the group element that yields the maximum activation:

$$a_g = \arg \max_{g \in C_4} \text{GlobalPool}(f_{\text{eq}}(g \cdot I)). \quad (15)$$

This direct approach provides a computationally efficient and theoretically principled method for canonicalization.

Non-Equivariant Network (Optimization-Based Canonicalization). In contrast to the direct prediction of the equivariant network, the non-equivariant approach achieves canonicalization through an optimization-based process. This method can leverage any standard backbone architecture, such as a conventional CNN or a pre-trained ResNet.

The non-equivariant network $f_{\text{non-eq}}$ operates by processing each transformed image in the input's orbit $\mathcal{T} = g_i \cdot I \mid g_i \in C_4$ to extract a corresponding feature representation $f g_i \in \mathbb{R}^d$. The optimal canonical transformation, g_{est} , is then identified by computing cosine similarities between extracted features and a learned reference vector $\mathbf{v}_{\text{ref}} \in \mathbb{R}^d$:

$$g_{\text{est}} = \arg \max_{g \in C_4} \frac{\mathbf{f} g^T \mathbf{v}_{\text{ref}}}{\|\mathbf{f} g\| \|\mathbf{v}_{\text{ref}}\|}, \quad (16)$$

where $\mathbf{f} g = f_{\text{non-eq}}(g \cdot I)$. The reference vector \mathbf{v}_{ref} is learned during training to encode the canonical feature distribu-

tion that optimizes task performance. This optimization-based canonicalization process enables our framework to leverage the powerful representational capabilities of established, non-equivariant architectures, thereby demonstrating its model-agnostic flexibility and broad applicability.

3.3. Action Invert Canonicalization

The action invert canonicalization finally transforms manipulation actions computed in canonical space back to the original workspace configuration. This process maintains the fundamental equivariance property that ensures spatial consistency throughout the entire manipulation pipeline, independent of the underlying architectural paradigm.

Given the estimated transformation g_{est} and policy outputs A_{canon} computed in canonical space, the inverse canonicalization operation applies the inverse group transformation to restore spatial alignment:

$$A_{\text{final}} = g_{\text{est}}^{-1} \cdot A_{\text{canon}}. \quad (17)$$

This formulation ensures that spatial relationships encoded in canonical representations are correctly mapped back to the original coordinate system, maintaining equivariance throughout the entire manipulation pipeline.

The practical implementation operates through a systematic transformation process that adapts to heterogeneous action representations across different manipulation frameworks. For CNN-based systems generating spatial probability distributions, the inverse canonicalization transforms feature maps through geometric operations. For Transformer-based models producing discrete action tokens or continuous action parameters, the transformation applies to the underlying spatial coordinates encoded within the action representations.

3.4. Equivariance Proof of Group Equivariant Canonicalization Framework

This section provides rigorous mathematical proofs demonstrating that our group equivariant canonicalization framework maintains equivariance properties throughout the entire manipulation pipeline.

Framework Equivariance. Let G be a finite group acting on input space \mathcal{X} and output space \mathcal{Y} . Given canonicalization function $C : \mathcal{X} \rightarrow \mathcal{X}$, base policy $\pi_{\text{base}} : \mathcal{X} \times \mathcal{L} \rightarrow \mathcal{Y}$, and inverse canonicalization $C^{-1} : \mathcal{Y} \rightarrow \mathcal{Y}$, the canonicalized policy:

$$\pi_{\text{canon}}(x, \ell) = C^{-1}(g_{\text{est}}) \cdot \pi_{\text{base}}(C(x), \ell), \quad (18)$$

is G -equivariant, where $C^{-1}(g_{\text{est}})$ represents the inverse canonicalization operation that applies the estimated transformation g_{est} to map canonical space outputs back to the original coordinate system. For any group element $g \in G$ and input $(x, \ell) \in \mathcal{X} \times \mathcal{L}$, we need to demonstrate that:

$$\pi_{\text{canon}}(g \cdot x, \ell) = g \cdot \pi_{\text{canon}}(x, \ell). \quad (19)$$

Proof. The proof relies on the fundamental property that all spatially equivalent inputs map to the same canonical representation, ensuring that $C(g \cdot x) = C(x) = x_{\text{canon}}$. This equivariance, combined with the transformation relationship $g'_{\text{est}} = g \cdot g_{\text{est}}$ (where g'_{est} denotes the estimated transformation for the transformed input $g \cdot x$), establishes the desired equivariance property. The complete mathematical derivations are provided in the Appendix.

For the transformed input $g \cdot x$:

$$\begin{aligned} \pi_{\text{canon}}(g \cdot x, \ell) &= C^{-1}(g'_{\text{est}}) \cdot \pi_{\text{base}}(C(g \cdot x), \ell) \\ &= g'_{\text{est}} \cdot \pi_{\text{base}}(x_{\text{canon}}, \ell) \\ &= (g \cdot g_{\text{est}}) \cdot \pi_{\text{base}}(x_{\text{canon}}, \ell) \\ &= g \cdot (g_{\text{est}} \cdot \pi_{\text{base}}(x_{\text{canon}}, \ell)) \\ &= g \cdot \pi_{\text{canon}}(x, \ell). \end{aligned} \quad (20)$$

This mathematical derivation demonstrates that our canonicalization framework systematically transforms arbitrary base policies into equivariant policies without architectural modifications, preserving spatial consistency while maintaining the representational strengths of existing manipulation architectures.

4. Experiments

To validate the effectiveness and universality of the proposed Eq.Bot framework, we conduct a series of comprehensive experiments to answer the following questions:

RQ1: How effectively does **Eq.Bot** work on both CNN-based and Transformer-based backbones?

RQ2: How does **Eq.Bot** perform under both simulation and real-world robotic manipulation scenarios?

RQ3: How does **Eq.Bot** perform on both seen and unseen robotic manipulation tasks?

RQ4: How does **Eq.Bot** perform with different canonicalization networks?

RQ5: How does **Eq.Bot** perform under different hyperparameter values?

4.1. Experimental Setup

This section introduces the experimental settings from tasks and baselines, while other details refer to the Appendix.

4.1.1. Environments and Tasks

Our experiments are conducted across both simulated and real-world environments to validate the effectiveness and generalization capabilities of our framework.

Simulation Environments. For CNN-based architectures, we utilize the Ravens [38] benchmark within the PyBullet [5] simulator. We evaluate performance on 18 language-conditioned manipulation tasks that demand precise spatial reasoning. For Transformer-based architectures, we employ the LIBERO [24] benchmark, which features four distinct task suites (Spatial, Object, Goal, and Long) designed

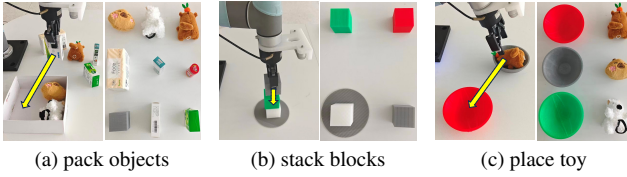


Figure 3. Real-world Tasks. Three robotic tabletop tasks are used for evaluation: (1) pack objects, (2) stack blocks, and (3) place toy. Each sub-figure displays the robot’s action (left) and the corresponding objects (right).

to assess a model’s compositional generalization and long-horizon reasoning abilities.

Real-World Environment. To assess the practical applicability and few-shot transfer of our framework, we conducted experiments on a physical UR5e robot. As illustrated in Figure 3, we designed three tabletop manipulation tasks: (1) *pack objects*, requiring the robot to place multiple small objects into a container; (2) *stack blocks*, which involves stacking two blocks in a specified order from arbitrary initial poses; and (3) *place toy*, where a toy must be placed into a designated bowl. For each task, all policies were trained using only 10 real-world demos under both *seen* and *unseen* conditions.

4.1.2. Baselines

To rigorously evaluate the performance of Eq.Bot, we compare it against a suite of relevant baselines for each architectural paradigm. For the CNN-based CLIPort experiments, we compare against: (1) Transporter-only [38], a purely spatial reasoning model; (2) CLIP-only [31], which relies solely on semantic understanding; (3) RN50-BERT [8, 13], a standard multi-modal fusion model; and (4) the original CLIPort [34] architecture. For the Transformer-based OpenVLA-OFT experiments, our comparisons include: (1) $\pi_0 + \text{FAST}$ [30], representing accelerated fine-tuning; (2) π_0 (fine-tuned) [1], indicating foundational performance; and (3) the original OpenVLA-OFT [20] model.

4.2. Analysis of Effectiveness and Universality

This section provides detailed analysis of Eq.Bot’s effectiveness under all kinds of conditions to answer **RQ1-RQ3**.

RQ1: Our results indicate that Eq.Bot serves as an effective module for enhancing both CNN-based and Transformer-based manipulation policies, albeit with varying degrees of improvement. As illustrated in our simulation and real-world results (Tables 1 and 2), the performance enhancement is particularly pronounced for the CNN-based CLIPort architecture. For instance, on the challenging put-blocks-in-bowls-unseen-colors task (1000 demos), Eq.Bot (GNet) boosts the success rate from 18.5% to 52.2%. This dramatic improvement is likely because CNNs inherently lack mechanisms to handle rotational variations, making

them highly susceptible to spatial equivariance errors. In contrast, for the Transformer-based OpenVLA-OFT model, which already possesses a more robust internal representation of spatial relationships, the improvements are more modest but still consistent across tasks.

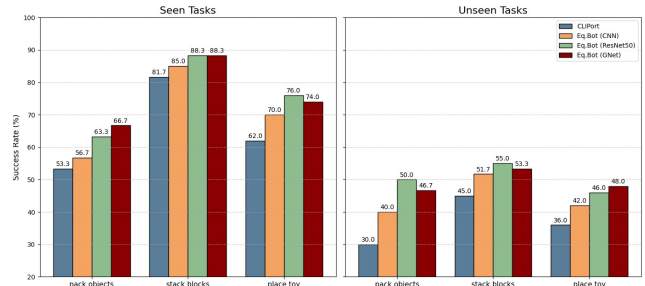


Figure 4. Real-world results. We compare our Eq.Bot variants with the original CLIPort baseline, showing performance on both seen (in-distribution) and unseen (out-of-distribution) tasks.

RQ2: Eq.Bot demonstrates strong performance and clear advantages in both simulated and real-world settings. In the structured and repeatable environments of the Ravens and LIBERO benchmarks, the framework consistently elevates the baseline success rates. However, the most significant impact is observed in the real-world experiments. Physical environments introduce a higher degree of variability, including subtle changes in lighting, object texture, and camera perspective, which can degrade the performance of base models. Eq.Bot’s ability to standardize the input observation before policy inference proves crucial in this context, leading to a marked improvement in robustness and task success. For instance, in the unseen pack objects task, Eq.Bot (ResNet50) achieves a 50.0% success rate, a 66.7% relative improvement over the baseline’s 30.0%, as illustrated in Figure 4. This highlights the framework’s practical utility in bridging the sim-to-real gap by mitigating the effects of unpredictable, real-world spatial variations.

RQ3: The framework exhibits excellent generalization to both seen and unseen conditions, with the most compelling results emerging in the unseen scenarios. For seen tasks, with the object poses and configurations similar, Eq.Bot provides a solid performance boost. The true strength of our approach, however, is revealed when the robot is presented with novel object conditions not encountered during training. For example, in the put-blocks-in-bowls task (1000 demos), while both the baseline CLIPort and Eq.Bot achieve a perfect 100% success rate under seen conditions, the baseline’s performance plummets to just 18.5% in the unseen setting. In stark contrast, Eq.Bot (GNet) maintains a robust 52.2% success rate, showcasing its vastly superior generalization capability. This confirms that our canonicalization approach does not simply memorize training configurations but imparts a systematic understanding of geometric equiv-

Table 1. Performance Comparisons on the CNN-based models. We compare our Eq.Bot variants with established baselines across a range of tasks with both **seen** and **unseen** object configurations. The primary metric is the task success rate (%), averaged over 100 evaluation trials for each task, conditioned on 1, 10, 100, or 1000 demos.

Method	packing-box-pairs				packing-box-pairs				packing-seen-google				packing-unseen-google				packing-seen-google				packing-unseen-google			
	seen-colors		unseen-colors		objects-seq		objects-seq		objects-seq		objects-seq		objects-group		objects-group		objects-group		objects-group		objects-group		objects-group	
	1	10	100	1000	1	10	100	1000	1	10	100	1000	1	10	100	1000	1	10	100	1000	1	10	100	1000
Transporter-only	44.2	55.2	54.2	52.4	34.6	48.7	47.2	54.1	26.2	39.7	45.4	46.3	19.9	29.8	28.7	37.3	60.0	54.3	61.5	59.9	46.2	54.7	49.8	52.0
CLIP-only	38.6	69.7	88.5	87.1	33.0	65.5	68.8	61.2	29.1	67.9	89.3	95.8	37.1	49.4	60.4	57.8	52.5	62.0	89.6	92.7	43.4	65.9	73.1	70.0
RN50-BERT	36.2	64.0	94.7	90.3	31.4	52.7	65.6	72.1	32.9	48.4	87.9	94.0	29.3	48.5	48.3	56.1	46.4	52.9	76.5	86.4	43.2	52.0	66.3	73.7
CLIPort	46.1	71.2	88.5	97.6	38.1	54.7	64.5	71.5	11.2	51.0	80.3	93.2	23.4	44.3	59.6	61.6	45.6	60.7	81.2	92.9	47.9	57.3	72.0	72.6
Eq.Bot (CNN)	50.8	74.9	93.7	99.1	45.8	67.3	74.2	75.3	14.7	56.0	87.9	96.7	30.8	45.3	62.7	72.3	47.8	64.9	87.2	96.7	50.7	59.2	77.2	76.5
Eq.Bot (ResNet50)	53.9	75.1	94.5	98.9	47.1	69.0	74.7	77.2	15.8	57.5	89.2	97.3	33.5	45.9	62.9	73.2	49.3	65.2	88.2	97.6	50.1	59.8	80.6	77.3
Eq.Bot (GNet)	54.3	76.5	95.2	99.0	46.7	71.8	78.1	78.8	16.4	58.2	89.4	97.3	32.1	47.3	63.3	73.5	50.2	67.1	90.1	97.5	51.3	60.3	80.9	79.2
Method	stack-block-pyramid				stack-block-pyramid				separating-piles				separating-piles				towers-of-hanoi				towers-of-hanoi			
	seq-seen-colors		seq-unseen-colors		seen-colors		unseen-colors		seq-seen-colors		seq-unseen-colors		seq-seen-colors		seq-unseen-colors		seq-seen-colors		seq-unseen-colors		seq-seen-colors		seq-unseen-colors	
	1	10	100	1000	1	10	100	1000	1	10	100	1000	1	10	100	1000	1	10	100	1000	1	10	100	1000
Transporter-only	4.5	2.3	5.2	4.5	3.0	4.0	2.3	5.8	42.7	52.3	42.0	48.4	41.2	49.2	44.7	52.3	25.4	67.9	98.0	99.9	24.3	44.6	71.7	80.7
CLIP-only	6.3	28.7	55.7	54.8	2.0	12.2	18.3	19.5	43.5	55.0	84.9	90.2	59.9	49.6	73.0	71.0	9.4	52.6	88.6	45.3	24.7	47.0	67.0	58.0
RN50-BERT	5.3	35.0	89.0	97.5	6.2	12.2	21.5	30.7	31.8	47.8	46.5	46.5	33.4	44.4	41.3	44.9	28.0	66.1	91.3	92.1	17.4	75.1	85.3	89.3
CLIPort	17.4	44.7	87.9	96.8	8.9	21.7	29.5	26.5	45.8	53.5	86.0	96.5	42.3	49.2	72.1	74.2	47.4	74.9	96.7	98.6	43.3	84.6	94.0	99.1
Eq.Bot (CNN)	21.5	52.3	92.0	99.5	14.1	27.8	30.2	34.0	51.7	58.7	94.9	98.0	43.8	56.2	75.3	82.1	53.8	83.9	99.7	100	41.9	85.3	99.7	100
Eq.Bot (ResNet50)	24.0	53.7	94.2	99.5	17.3	30.5	33.0	31.5	53.2	60.9	94.1	98.1	46.1	58.2	75.6	79.6	56.2	86.0	100	100	42.7	84.7	99.9	100
Eq.Bot (GNet)	24.6	54.2	95.0	99.0	18.5	28.5	34.0	29.8	52.8	61.5	93.2	98.3	47.3	58.9	77.1	79.3	57.6	85.3	100	100	43.8	83.2	99.7	100
Method	align-rope				packing-unseen-shapes				assembling-kits-seq				assembling-kits-seq				put-blocks-in-bowls				put-blocks-in-bowls			
	seen-colors		unseen-colors		seen-colors		unseen-colors		seen-colors		unseen-colors		seen-colors		unseen-colors		seen-colors		unseen-colors		seen-colors		unseen-colors	
	1	10	100	1000	1	10	100	1000	1	10	100	1000	1	10	100	1000	1	10	100	1000	1	10	100	1000
Transporter-only	6.9	30.6	33.1	51.5	16.0	20.0	22.0	22.0	5.8	11.6	28.6	29.6	7.8	17.6	25.6	28.4	16.8	33.3	62.7	64.7	11.7	17.2	14.8	18.7
CLIP-only	13.4	48.7	70.4	70.7	13.0	28.0	44.0	50.0	0.8	9.2	19.8	23.0	2.0	4.6	10.8	19.8	23.5	60.2	93.5	97.7	11.2	34.2	33.2	44.5
RN50-BERT	3.1	25.0	63.8	57.1	19.0	25.0	32.0	44.0	2.2	5.6	11.6	21.8	1.6	6.4	10.4	18.4	13.8	44.5	81.2	91.8	16.2	23.0	30.3	23.8
CLIPort	15.9	48.6	62.4	90.6	22.0	28.0	32.0	38.0	9.8	14.2	36.8	53.2	12.6	17.4	33.6	31.0	20.4	38.3	91.2	100	16.0	29.0	37.1	18.5
Eq.Bot (CNN)	22.8	58.6	91.5	93.1	23.0	40.0	48.0	50.0	12.8	17.8	47.0	52.4	16.6	19.6	33.8	31.2	30.1	51.2	98.8	100	18.7	30.2	54.7	51.2
Eq.Bot (ResNet50)	23.5	62.6	92.6	94.5	25.0	38.0	50.0	54.0	13.6	18.3	48.2	53.6	18.2	21.6	32.0	30.4	31.5	52.7	99.5	100	19.5	32.7	59.8	52.3
Eq.Bot (GNet)	24.1	64.9	93.6	96.2	24.0	44.0	51.0	55.0	13.2	19.4	51.6	54.8	17.8	22.4	31.0	33.0	32.7	53.2	99.8	100	20.3	32.5	58.5	52.2

Table 2. Performance Comparisons on the Transformer-based Models. We compare our Eq.Bot variants (integrated with OpenVLA-OFT) with the original model and other fine-tuning baselines on the LIBERO benchmark. Results are averaged over multiple trials for each of the four official task suites.

Method	Spatial	Object	Goal	Long	Average
π_0 + FAST (fine-tuned)	96.4	96.8	88.6	60.2	85.5
π_0 (fine-tuned)	96.8	98.8	95.8	85.2	94.2
OpenVLA-OFT	96.6	97.8	97.6	94.1	96.5
Eq.Bot (CNN)	97.4	98.2	97.8	94.6	97.0
Eq.Bot (ResNet50)	97.9	98.6	98.4	95.1	97.5
Eq.Bot (GNet)	98.1	98.8	98.5	95.2	97.7

alence, enabling the policy to generalize its learned skills to a wider range of spatial arrangements.

4.3. Canonicalization Network Analysis (RQ4)

As introduced in Section 3.2, the canonicalization network can be instantiated with different architectures. Results reveal that the choice of architecture has a significant impact on performance, with the GNet variant consistently demonstrating the most robust and superior results. For example, on the packing-unseen-google-objects-group task (100 demos) of CLIPort, Eq.Bot (GNet) achieves a success rate of 80.9%, outperforming both the ResNet-50 (80.6%) and standard CNN (77.2%) variants. This indicates that explici-

itly embedding geometric priors through its equivariant architecture allows it to identify the canonical orientation with greater accuracy and reliability. While the ResNet-50 and standard CNN variants also provide substantial improvements over the baselines, they consistently underperform the more specialized GNet in aggregate. Although there are instances where they are competitive—for example, on the assembling-kits-seq task (100 demos) with unseen colors, the CNN variant achieves 33.8% compared to GNet’s 31.0%—GNet’s strong average performance and clear superiority in the most complex, out-of-distribution scenarios highlight its superior generalization. These results strongly suggest that incorporating the correct inductive biases for the task is more critical than simply increasing model size.

4.4. Hyperparameter Analysis (RQ5)

A key hyperparameter in our framework is the order N of the discrete rotation group C_N . This parameter dictates the granularity of the rotational search space; a larger N allows for a finer search at the expense of increased computation.

The results, summarized in Table 3, reveal that while performance is remarkably stable across both group orders, the coarser C_4 discretization consistently achieves slightly better results in most scenarios. For instance, in the challenging assemble unseen kits task with 10 demos, Eq.Bot (GNet) with C_4 achieves a 22.4% success rate, outperform-

Table 3. Ablation on discrete rotation group order (C_4 vs. C_8). We compare our three Eq.Bot variants on four Ravens benchmark tasks across seen/unseen tasks. Each model is trained with 10 or 100 demos for various group configuration (C_4 and C_8).

Method	pack seen objects				assemble seen kits			
	C_4		C_8		C_4		C_8	
	10	100	10	100	10	100	10	100
Eq.Bot (CNN)	56.0	87.9	55.5	86.5	17.8	47.0	16.8	44.2
Eq.Bot (ResNet-50)	57.5	89.2	57.0	87.6	18.3	48.2	18.0	46.0
Eq.Bot (GNet)	58.2	89.4	57.6	87.8	19.4	51.6	18.7	49.3
Method	pack unseen objects				assemble unseen kits			
	C_4		C_8		C_4		C_8	
	10	100	10	100	10	100	10	100
Eq.Bot (CNN)	45.3	62.7	43.9	62.8	19.6	33.8	18.4	30.2
Eq.Bot (ResNet-50)	45.9	62.9	44.6	62.4	21.6	32.0	19.6	29.8
Eq.Bot (GNet)	47.3	63.3	46.5	62.5	22.4	31.0	20.7	30.4

ing its C_8 counterpart (20.7%). This trend generally holds across both seen and unseen tasks, as well as in low-data and high-data regimes. We hypothesize that while C_8 offers a more precise canonical representation, it also frames canonicalization as a more difficult classification problem for the network. Especially in the low-data regime, the network may struggle to robustly predict the correct orientation among eight fine-grained classes. Above all, our framework can achieve comparable performance under C_4 , which indicates that it has provided a sufficient geometric prior.

5. Related Work

Development of Robotic Learning Frameworks: Early robotic manipulation systems mainly relied on pre-programmed control and precise kinematic modeling [6], struggling to adapt in complex environments. The advent of reinforcement learning (RL) [21] introduced trial-and-error paradigms, but suffered from sample inefficiency and safety risks. Imitation learning subsequently emerged as a data-driven alternative, enabling robots to learn policies directly from expert demonstrations [15]. However, this paradigm remains susceptible to distribution mismatch, demonstration quality dependency, and covariate shift issues. More recently, multi-modal frameworks that integrate visual, linguistic, and action information have facilitated more intuitive human-robot interaction [27]. Despite these advancements, these multi-modal systems generally lack inherent equivariance properties and fail to robustly handle spatial transformations of manipulated objects.

Existing Approaches for Spatial Transformations: Traditional methods for handling spatial transformations primarily rely on geometric data augmentation, applying operations such as rotation, translation, and scaling during training [28]. While improving robustness, they increase computational overhead and cannot guarantee systematic

generalization. Recent developments have introduced more effective strategies: diffusion-based augmentation methods enable transformations by modifying object properties [10, 12]; multi-modal fusion approaches integrate complementary information from diverse sensor inputs [29, 40, 41]; spatial enhancement techniques improve 3D geometric understanding via graph-based modeling of joint dependencies [2, 35]. Yet a fundamental limitation persists: they either demand extensive computational resources or lack theoretical guarantees for spatial generalization.

Equivariance-based Approaches for Spatial Transformations: Early attempts using handcrafted features like SIFT [25] and HOG [7] provided empirical robustness to geometric transformations but lacked sufficient representational capacity. An innovative breakthrough occurred with Group Equivariant Convolutional Neural Networks (G-CNNs) [4], which systematically incorporated group theory into convolutional neural networks, thereby establishing theoretical foundations for equivariance networks.

Subsequent research has progressively extended equivariance to robotic manipulation. For instance, GEM [16] enforces geometric equivariance through language-steerable kernels and textual-visual correlation graphs. Similarly, EqvAfford [3] achieves point-level affordance learning with geometric equivariance. ET-seed [36] adopts a trajectory-level equivariant diffusion policy, modeling actions directly on the transformation manifold. EquAct [42] further instantiates continuous equivariance within transformer architectures, ensuring equivariant keyframe predictions. However, these equivariance-based approaches typically demand substantial architectural modifications and are difficult to port across different models, motivating the development of more flexible and model-agnostic methods that can enhance spatial equivariance while preserving the representational benefits of existing architectures.

6. Conclusion

We propose Eq.Bot, a universal and model-agnostic canonicalization framework grounded in group equivariant theory, enhancing spatial equivariance to existing manipulation systems. Instead of requiring bespoke and complex architectural modifications, Eq.Bot seamlessly integrates with existing policies by transforming observations into a canonical orientation, leveraging an unmodified base policy to predict actions, and then mapping these actions back to the original coordinate frame. This approach is not only effective but also highly flexible, supporting diverse canonicalization networks, from inherently equivariant G-CNNs to optimization-based methods using standard backbones. Extensive experiments demonstrated that Eq.Bot significantly enhances the performance and robustness of both CLIPort and OpenVLA-OFT across a variety of manipulation tasks, validating our framework’s effectiveness and universality.

References

[1] Kevin Black, Noah Brown, Danny Driess, Adnan Esmail, Michael Equi, Chelsea Finn, Niccolò Fusai, Lachy Groom, Karol Hausman, Brian Ichter, et al. π_0 : A vision-language-action flow model for general robot control. *arXiv preprint arXiv:2410.24164*, 2024. 6

[2] Yujun Cai, Liuhan Ge, Jun Liu, Jianfei Cai, Tat-Jen Cham, Junsong Yuan, and Nadia Magnenat Thalmann. Exploiting spatial-temporal relationships for 3d pose estimation via graph convolutional networks. In *Proceedings of the IEEE/CVF international conference on computer vision*, pages 2272–2281, 2019. 8

[3] Yue Chen, Chenrui Tie, Ruihai Wu, and Hao Dong. Eqvaford: Se (3) equivariance for point-level affordance learning. *arXiv preprint arXiv:2408.01953*, 2024. 8

[4] Taco Cohen and Max Welling. Group equivariant convolutional networks. In *International conference on machine learning*, pages 2990–2999. PMLR, 2016. 2, 8

[5] Erwin Coumans and Yunfei Bai. Pybullet, a python module for physics simulation for games, robotics and machine learning, 2016. 5

[6] John J Craig. *Introduction to robotics: mechanics and control, 3/E*. Pearson Education India, 2009. 8

[7] Navneet Dalal and Bill Triggs. Histograms of oriented gradients for human detection. In *2005 IEEE computer society conference on computer vision and pattern recognition (CVPR'05)*, pages 886–893. Ieee, 2005. 8

[8] Jacob Devlin, Ming-Wei Chang, Kenton Lee, and Kristina Toutanova. Bert: Pre-training of deep bidirectional transformers for language understanding. In *Proceedings of the 2019 conference of the North American chapter of the association for computational linguistics: human language technologies, volume 1 (long and short papers)*, pages 4171–4186, 2019. 6

[9] Guoguang Du, Kai Wang, Shiguo Lian, and Kaiyong Zhao. Vision-based robotic grasping from object localization, object pose estimation to grasp estimation for parallel grippers: a review. *Artificial Intelligence Review*, 54(3):1677–1734, 2021. 1

[10] Lisa Dunlap, Alyssa Umino, Han Zhang, Jiezhi Yang, Joseph E Gonzalez, and Trevor Darrell. Diversify your vision datasets with automatic diffusion-based augmentation. *Advances in neural information processing systems*, 36:79024–79034, 2023. 8

[11] Morton Hamermesh. *Group theory and its application to physical problems*. Courier Corporation, 2012. 2

[12] Haoran He, Chenjia Bai, Kang Xu, Zhuoran Yang, Weinan Zhang, Dong Wang, Bin Zhao, and Xuelong Li. Diffusion model is an effective planner and data synthesizer for multi-task reinforcement learning. *Advances in neural information processing systems*, 36:64896–64917, 2023. 8

[13] Kaiming He, Xiangyu Zhang, Shaoqing Ren, and Jian Sun. Deep residual learning for image recognition. In *Proceedings of the IEEE conference on computer vision and pattern recognition*, pages 770–778, 2016. 6

[14] Haojie Huang, Dian Wang, Arsh Tangri, Robin Walters, and Robert Platt. Leveraging symmetries in pick and place. *The International Journal of Robotics Research*, 43(4):550–571, 2024. 2

[15] Ahmed Hussein, Mohamed Medhat Gaber, Eyad Elyan, and Chrisina Jayne. Imitation learning: A survey of learning methods. *ACM Computing Surveys (CSUR)*, 50(2):1–35, 2017. 8

[16] Mingxi Jia, Haojie Huang, Zhewen Zhang, Chenghao Wang, Linfeng Zhao, Dian Wang, Jason Xinyu Liu, Robin Walters, Robert Platt, and Stefanie Tellex. Learning efficient and robust language-conditioned manipulation using textual-visual relevancy and equivariant language mapping. *IEEE Robotics and Automation Letters*, 2025. 1, 8

[17] Sékou-Oumar Kaba, Arnab Kumar Mondal, Yan Zhang, Yoshua Bengio, and Siamak Ravaniabakhsh. Equivariance with learned canonicalization functions. In *International Conference on Machine Learning*, pages 15546–15566. PMLR, 2023. 3

[18] Artúr István Károly, Péter Galambos, József Kuti, and Imre J Rudas. Deep learning in robotics: Survey on model structures and training strategies. *IEEE Transactions on Systems, Man, and Cybernetics: Systems*, 51(1):266–279, 2020. 1

[19] Adalbert Kerber. *Applied finite group actions*. Springer Science & Business Media, 2013. 2

[20] Moo Jin Kim, Chelsea Finn, and Percy Liang. Fine-tuning vision-language-action models: Optimizing speed and success. *arXiv preprint arXiv:2502.19645*, 2025. 1, 6, 2

[21] Jens Kober, J Andrew Bagnell, and Jan Peters. Reinforcement learning in robotics: A survey. *The International Journal of Robotics Research*, 32(11):1238–1274, 2013. 8

[22] Oliver Kroemer, Scott Niekum, and George Konidaris. A review of robot learning for manipulation: Challenges, representations, and algorithms. *Journal of machine learning research*, 22(30):1–82, 2021. 1

[23] Karel Lenc and Andrea Vedaldi. Understanding image representations by measuring their equivariance and equivalence. In *Proceedings of the IEEE conference on computer vision and pattern recognition*, pages 991–999, 2015. 2

[24] Bo Liu, Yifeng Zhu, Chongkai Gao, Yihao Feng, Qiang Liu, Yuke Zhu, and Peter Stone. Libero: Benchmarking knowledge transfer for lifelong robot learning. *Advances in Neural Information Processing Systems*, 36:44776–44791, 2023. 5

[25] David G Lowe. Object recognition from local scale-invariant features. In *Proceedings of the seventh IEEE international conference on computer vision*, pages 1150–1157. Ieee, 1999. 8

[26] Kevin M Lynch and Frank C Park. *Modern robotics*. Cambridge University Press, 2017. 1

[27] Yueen Ma, Zixing Song, Yuzheng Zhuang, Jianye Hao, and Irwin King. A survey on vision-language-action models for embodied ai. *arXiv preprint arXiv:2405.14093*, 2024. 8

[28] Kiran Maharana, Surajit Mondal, and Bhushankumar Neemade. A review: Data pre-processing and data augmentation techniques. *Global Transitions Proceedings*, 3(1):91–99, 2022. 8

[29] Xiaomin Ouyang, Xian Shuai, Jiayu Zhou, Ivy Wang Shi, Zhiyuan Xie, Guoliang Xing, and Jianwei Huang. Cosmo: contrastive fusion learning with small data for multimodal

human activity recognition. In *Proceedings of the 28th Annual International Conference on Mobile Computing And Networking*, pages 324–337, 2022. 8

[30] Karl Pertsch, Kyle Stachowicz, Brian Ichter, Danny Driess, Suraj Nair, Quan Vuong, Oier Mees, Chelsea Finn, and Sergey Levine. Fast: Efficient action tokenization for vision-language-action models. *arXiv preprint arXiv:2501.09747*, 2025. 6

[31] Alec Radford, Jong Wook Kim, Chris Hallacy, Aditya Ramesh, Gabriel Goh, Sandhini Agarwal, Girish Sastry, Amanda Askell, Pamela Mishkin, Jack Clark, et al. Learning transferable visual models from natural language supervision. In *International conference on machine learning*, pages 8748–8763. PMLR, 2021. 6

[32] Roger N Shepard and Jacqueline Metzler. Mental rotation of three-dimensional objects. *Science*, 171(3972):701–703, 1971. 2

[33] Connor Shorten and Taghi M Khoshgoftaar. A survey on image data augmentation for deep learning. *Journal of big data*, 6(1):1–48, 2019. 1

[34] Mohit Shridhar, Lucas Manuelli, and Dieter Fox. Cliport: What and where pathways for robotic manipulation. In *Conference on robot learning*, pages 894–906. PMLR, 2022. 1, 6, 2

[35] Chenyang Si, Wentao Chen, Wei Wang, Liang Wang, and Tieniu Tan. An attention enhanced graph convolutional lstm network for skeleton-based action recognition. In *Proceedings of the IEEE/CVF conference on computer vision and pattern recognition*, pages 1227–1236, 2019. 8

[36] Chenrui Tie, Yue Chen, Ruihai Wu, Boxuan Dong, Zeyi Li, Chongkai Gao, and Hao Dong. Et-seed: Efficient trajectory-level se (3) equivariant diffusion policy. *arXiv preprint arXiv:2411.03990*, 2024. 8

[37] Maurice Weiler and Gabriele Cesa. General e (2)-equivariant steerable cnns. *Advances in neural information processing systems*, 32, 2019. 4

[38] Andy Zeng, Pete Florence, Jonathan Tompson, Stefan Welker, Jonathan Chien, Maria Attarian, Travis Armstrong, Ivan Krasin, Dan Duong, Vikas Sindhwani, et al. Transporter networks: Rearranging the visual world for robotic manipulation. In *Conference on Robot Learning*, pages 726–747. PMLR, 2021. 5, 6

[39] Fanlong Zeng, Wensheng Gan, Yongheng Wang, Ning Liu, and Philip S Yu. Large language models for robotics: A survey. *arXiv preprint arXiv:2311.07226*, 2023. 1

[40] Yanan Zhang, Jiaxin Chen, and Di Huang. Cat-det: Contrastively augmented transformer for multi-modal 3d object detection. In *Proceedings of the IEEE/CVF Conference on Computer Vision and Pattern Recognition*, pages 908–917, 2022. 8

[41] Fei Zhao, Chengcui Zhang, and Baocheng Geng. Deep multimodal data fusion. *ACM computing surveys*, 56(9):1–36, 2024. 8

[42] Xupeng Zhu, Yu Qi, Yizhe Zhu, Robin Walters, and Robert Platt. Equact: An se (3)-equivariant multi-task transformer for open-loop robotic manipulation. *arXiv preprint arXiv:2505.21351*, 2025. 1, 8

APPENDIX A: Theoretical Derivation for the Eq.Bot Framework

This appendix provides a detailed mathematical derivation for the **Eq.Bot** framework, establishing the theoretical foundation for its equivariance guarantees.

A.1 Canonicalization Processing

The canonicalization process firstly maps an input observation x to a standardized canonical representation x_{canon} . This is achieved by applying the inverse of an estimated transformation g_{est} predicted by a canonicalization network C_{net} . The canonicalization function $C(x)$ is defined as:

$$C(x) = (g_{\text{est}})^{-1} \cdot x = x_{\text{canon}}, \quad (21)$$

where $g_{\text{est}} = C_{\text{net}}(x)$ transforms x into the canonical frame.

A fundamental property of our framework is that all spatially equivalent inputs are mapped to the *same* canonical representation. Consider an input x transformed by an arbitrary group element $g \in G$. The new, transformed input is $g \cdot x$. The canonicalization network will process this new input and estimate a new transformation, g'_{est} :

$$g'_{\text{est}} = C_{\text{net}}(g \cdot x), \quad (22)$$

The canonical representation of the transformed input is:

$$C(g \cdot x) = (g'_{\text{est}})^{-1} \cdot (g \cdot x), \quad (23)$$

Since the canonical representation is invariant to the initial transformation g , we have $C(g \cdot x) = C(x)$, then:

$$(g'_{\text{est}})^{-1} \cdot (g \cdot x) = (g_{\text{est}})^{-1} \cdot x, \quad (24)$$

By right-multiplying both sides by x^{-1} (in the context of the group action) and rearranging, we get:

$$\begin{aligned} (g'_{\text{est}})^{-1} \cdot g &= (g_{\text{est}})^{-1} \\ g'_{\text{est}} \cdot (g'_{\text{est}})^{-1} \cdot g &= g'_{\text{est}} \cdot (g_{\text{est}})^{-1} \\ g &= g'_{\text{est}} \cdot (g_{\text{est}})^{-1} \\ g \cdot g_{\text{est}} &= g'_{\text{est}}. \end{aligned} \quad (25)$$

This relationship demonstrates that when the input x is transformed by g , the estimated canonical transformation adjusts by the same group element, ensuring consistency in the canonicalization process.

A.2 Base Policy Processing in Canonical Space

For an original input x and a language instruction ℓ , the base policy π_{base} (e.g., CLIPort or OpenVLA-OFT) produces a canonical action A_{canon} :

$$\pi_{\text{base}}(C(x), \ell) = \pi_{\text{base}}(x_{\text{canon}}, \ell) = A_{\text{canon}}, \quad (26)$$

Now, considering the transformed input $g \cdot x$, the base policy receives $C(g \cdot x)$ as input. As established in the previous section, all group-equivalent inputs are mapped to the identical canonical form x_{canon} , i.e., $C(g \cdot x) = x_{\text{canon}}$, we have:

$$\pi_{\text{base}}(C(g \cdot x), \ell) = \pi_{\text{base}}(x_{\text{canon}}, \ell) = A_{\text{canon}}. \quad (27)$$

This demonstrates that the output of the base policy is invariant to the initial transformation g , indicating that the base policy π_{base} **does not need to be equivariant itself**.

A.3 Action Inverse Canonicalization and Proof of Equivariance

Finally, the inverse canonicalization maps the action A_{canon} generated in the canonical space back to the original coordinate frame of the input observation, achieved by applying the estimated transformation g_{est} . The final action A_{final} is:

$$\begin{aligned} \pi_{\text{canon}}(x, \ell) &= g_{\text{est}} \cdot \pi_{\text{base}}(C(x), \ell) \\ &= g_{\text{est}} \cdot \pi_{\text{base}}((g_{\text{est}})^{-1} \cdot x, \ell), \end{aligned} \quad (28)$$

We now prove that this complete policy π_{canon} is G-equivariant. Let's start with the left-hand side of the equation, evaluating the policy on the transformed input $g \cdot x$:

$$\pi_{\text{canon}}(g \cdot x, \ell) = g'_{\text{est}} \cdot \pi_{\text{base}}(C(g \cdot x), \ell), \quad (29)$$

From our previous derivations, we have the known relationships: 1) $g'_{\text{est}} = g \cdot g_{\text{est}}$ (from Eq. 25), and 2) $C(g \cdot x) = x_{\text{canon}}$ (from the definition of canonicalization). Substituting these into the equation gives:

$$\pi_{\text{canon}}(g \cdot x, \ell) = (g \cdot g_{\text{est}}) \cdot \pi_{\text{base}}(x_{\text{canon}}, \ell), \quad (30)$$

Using the associativity property of group actions, we can re-group the terms:

$$\pi_{\text{canon}}(g \cdot x, \ell) = g \cdot (g_{\text{est}} \cdot \pi_{\text{base}}(x_{\text{canon}}, \ell)), \quad (31)$$

We recognize that the term in the parentheses, $g_{\text{est}} \cdot \pi_{\text{base}}(x_{\text{canon}}, \ell)$, is precisely the definition of our policy applied to the original input x , i.e., $\pi_{\text{canon}}(x, \ell)$ (from Eq. 28).

Therefore, we arrive at the final result:

$$\pi_{\text{canon}}(g \cdot x, \ell) = g \cdot \pi_{\text{canon}}(x, \ell). \quad (32)$$

This completes the proof and formally establishes that the **Eq.Bot** framework imparts G-equivariance to any arbitrary base policy π_{base} , providing a rigorous theoretical guarantee for its generalization across spatial transformations.

APPENDIX B: Experiment Details

This appendix provides a comprehensive overview of the implementation details, training protocols, and evaluation metrics of the experiments presented in the main paper.

B.1 Implementation Details

CLIPort Experiments All models within the CLIPort-based experiment were trained for 200,000 iterations on a single NVIDIA V100 GPU with 32GB of VRAM, using a batch size of 1. We set the learning rate for the base models (CLIPort) to 1×10^{-4} . For our canonicalization modules, a higher learning rate of 1×10^{-3} was employed to promote faster convergence of the canonicalization network.

OpenVLA-OFT Experiments In line with the official fine-tuning protocol for OpenVLA-OFT, all models were fine-tuned for 150,000 steps on two NVIDIA A100 GPUs (40GB VRAM each). We used a per-GPU batch size of 2, resulting in an effective batch size of 4. A unified learning rate of 5×10^{-4} was applied to both the base model and the canonicalization module, governed by a multi-step decay scheduler to ensure training stability.

Real-World Experimental Setup Our real-world evaluations were conducted using a UR5e robotic arm equipped with a Robotiq 2F-85 parallel gripper. To provide comprehensive visual information, the scene was captured from three distinct viewpoints using Intel RealSense D415 cameras. We designed three tabletop manipulation tasks to rigorously assess policy robustness against spatial transformations: **Pack Objects**, **Stack Blocks**, and **Place Toy**. To create a challenging few-shot learning scenario, each policy was trained using a small dataset of only 10 expert demonstrations collected via teleoperation.

B.2 Model Variants and Training Analysis

Canonicalization Network Variants Our framework’s versatility was evaluated by implementing three distinct canonicalization network architectures, each presenting unique trade-offs between parameter efficiency and representational capacity:

- **Eq.Bot (CNN):** A standard CNN architecture with 61M parameters.
- **Eq.Bot (ResNet-50):** A deeper ResNet-50-based architecture with 67M parameters.
- **Eq.Bot (GNet):** An exceptionally parameter-efficient group equivariant CNN with only 1M parameters, demonstrating its suitability for lightweight deployment.

For CLIPort, which uses a two-stream (pick and place) policy, the canonicalization module is applied to each stream, effectively doubling the parameter overhead (e.g., $1M \times 2$ for GNet).

Training and Inference Runtimes For CLIPort-based experiments, the original baseline model required approximately 2 days for training. Our canonicalization framework introduces a computational overhead during training, which

varies with the chosen network architecture. The non-equivariant variants, Eq.Bot (CNN) and Eq.Bot (ResNet-50), required 3 days of training, while the equivariant variant, Eq.Bot (GNet), necessitated a longer training cycle of approximately 5 days. This increased computational investment is a direct trade-off for the substantial improvements observed in spatial generalization and task success. A similar pattern emerged in the OpenVLA-OFT experiments. While the baseline models required 26–28 hours for fine-tuning, our canonicalized methods (including CNN, ResNet-50, and GNet variants) necessitated a modestly increased duration, ranging from 28 to 32 hours. This slight overhead is the necessary cost to unlock superior robustness against out-of-distribution spatial transformations. For both CLIPort and OpenVLA-OFT, the inference times were comparable across all baseline and canonicalized models.

B.3 Datasets and Evaluation Metrics

Datasets All experiments leverage publicly available datasets to ensure fair comparison.

- **Ravens:** For the Ravens benchmark, we utilized the demonstration data provided by the original CLIPort study [34]. Each task includes datasets of 1, 10, 100, and 1000 demonstrations.
- **LIBERO:** For the LIBERO benchmark, we adhered to the experimental protocol of OpenVLA-OFT [20], using the provided demonstration datasets for fine-tuning.
- **Real-World:** For our real-world experiments, we collected a small-scale dataset of 10 expert demonstrations for each of the three tasks.

Evaluation Metrics The primary metric across all experiments is the **success rate (%)**, defined as the percentage of trials in which the robot successfully completes the language-specified objective.

- **In Simulation:** For each task in the Ravens benchmark, policies were evaluated over 100 independent trials. For the LIBERO benchmark, each policy was evaluated over 500 trials per task.
- **In the Real World:** To assess performance under practical conditions, we conducted extensive physical evaluations. Policies were evaluated across 30 trials for the *Pack Objects* task, 60 trials for *Stack Blocks*, and 50 trials for *Place Toy*. All real-world evaluations were performed under both *seen* (in-distribution) and *unseen* (out-of-distribution) conditions to rigorously test generalization. The final reported metric is the average success rate across all trials for a given task and condition.